

# Numerical analysis of the axially loaded concrete filled steel tube columns with debonding separation at the steel-concrete interface

Chen Shiming\*<sup>1</sup> and Zhang Huifeng<sup>1,2</sup>

<sup>1</sup>*School of Civil Engineering, Tongji University, Shanghai, PRC, (200092), China*

<sup>2</sup>*Architectural Design and Research Institute of Tongji University, Shanghai, PRC, (200092), China*

*(Received December 21, 2011, Revised April 09, 2012, Accepted May 30, 2012)*

**Abstract.** The interaction between steel tube and concrete core is the key design considerations for concrete-filled steel tube columns. In a concrete-filled steel tube (CFST) column, the steel tube provides confinement to the concrete core which permits the composite action among the steel tube and the concrete. Due to construction faults and plastic shrinkage of concrete, the debonding separation at the steel-concrete interface weakens the confinement effect, and hence affects the behaviour and bearing capacity of the composite member. This study investigates the axial loading behavior of the concrete filled circular steel tube columns with debonding separation. A three-dimensional nonlinear finite element model of CFST composite columns with introduced debonding gap was developed. The results from the finite element analysis captured successfully the experimental behaviours. The calibrated finite element models were then utilized to assess the influence of concrete strength, steel yield stress and the steel-concrete ratio on the debonding behaviour. The findings indicate a likely significant drop in the load carrying capacity with the increase of the size of the debonding gap. A design formula is proposed to reduce the load carrying capacity with the presence of debonding separation.

**Keywords:** debonding separation; concrete filled steel tube; axial compression; load carrying capacity.

---

## 1. Introduction

Concrete filled steel tubes (CFST) are widely used in recent decades (Uy 1998, Hajjar 2003, Zhong 2006, Han and Li 2011). Recent applications of CFSTs within China include columns in braced frames of high-rise buildings and bearing arches in large span arch bridges. CFSTs have shown better structural performance such as strength, stiffness, and ductility than that of bare steel or reinforced concrete members. Conventionally, CFSTs are designated by the shape of the steel tube which includes rectangular, square, circular and elliptical hollow sections. For CFST columns of circular section (CCFST) in particular, the steel tube provides significant confinement to the concrete core, which leads to an increase in both strength and ductility of the concrete, while the steel tube also acts as permanent formwork as well as reinforcement for the concrete. The concrete core, in turn, restricts inward local buckling of the steel tube.

---

\* Corresponding author, Professor, E-mail: [chensm@tongji.edu.cn](mailto:chensm@tongji.edu.cn)

Interaction between the steel tube and the concrete is the key design aspect to understand the behaviour of the CFT composite columns. The structural benefits require continuous stress transfer between steel and concrete to ensure their composite action. In practice, this is normally attained by relying on either the shear connectors on the inside wall of the tubes or the natural bond between the steel and the concrete. Comprehensive experimental and analytical researches on concrete filled tubular steel columns have been ongoing throughout the world for many years and were reported in the literatures (Roeder *et al.* 1999, Ellobody *et al.* 2006, Gupta *et al.* 2007, Choi and Xiao 2010, Yin and Lu 2010). The majority of these experiments however have been on moderate scale specimens (CCFST for example, less than 200 mm in diameter) using normal and high-strength concrete. Experimental study also showed (Han and Yao 2003) that the concrete compaction would affect the interaction between the steel tube and the concrete core, and thus the behaviour of the composite columns. It was also found that with better compaction both microlocking and macrolocking could be enhanced resulting in higher member load-carrying capacities. Codes and design specifications have been evaluated and developed, more or less in an enormous dissimilarity in the analytical models for evaluating the strength of a CFST composite column and the effect of confinement. Specifically, the ACI provisions (ACI Committee 318 2011) assume that the capacity of a CFST column can be predicted by treating the column as an ordinary reinforced concrete column, while in AISC provisions (American Institute of Steel Construction 2010), the design philosophy is to create modified cross sectional properties from the composite column and then design the composite column as an equivalent steel column using the modified properties in place of the steel properties. For calculating the axial capacity, codes such as ACI and Japanese Standards (Architectural Institute of Japan 1997) do not take into consideration of the concrete confinement, while some such as Eurocode 4 (European Committee for Standardization, 2004) take the strength contribution from the concrete confinement.

Most researches carried out to date on concrete filled steel tubes are based on the assumption that there is inherent perfect interaction between the concrete and the steel tube (Liang and Fragomeni 2010, Uwe *et al.* 2010, Xu *et al.* 2010, Bahrami *et al.* 2011). In construction practice, however, defects like concrete inanity or debonding of the concrete from steel tube have been found at the steel-concrete interface of the concrete-filled steel tubes. Debonding separation at the steel concrete interface of a CFST composite member could be induced by plastic shrinkage, and long term effect of concrete like temperature, shrinkage and creep as well as improper concrete casting. Fig. 1 illustrates a severe defect of inanity found in the concrete filled steel tube of an arch bridge. These concrete defects would penalize the structural performance of the composite columns. Besides, some defects of inanity between the steel plate and the concrete are identified being inherent shortcomings of concrete casting



Fig. 1 A severe defect of inanity in the concrete filled steel tube of an arch bridge

owing to substantial plastic shrinkage in concrete. For example, the defects of inanity in concrete would likely occur inside the steel tube in a beam to column joint immediately underneath the inner steel plate which is used to stiffen the steel column in transferring the force from the flanges of steel beams. Continuity of the upper part and the lower part of concrete is stopped by the inner steel plate, when substantial plastic shrinkage occurs.

The negative influences of the debonding on the axial loading capacity of the CFST columns were investigated experimentally by Liu *et al.* (2011), Xue *et al.* (2010) and Mu *et al.* (2007).

The defects of inanity between the steel tube, steel plate and the concrete were found to affect the structural behaviour and performance of the concrete filled steel tubes. The ultimate load capacity and the ductility of the CFSTs were also found significantly decreased with an increase of the debonding separation gap. In the CFST column construction practice, using low shrinkage concrete or even self-compact concrete is one way to improve the construction quality, but more or less, the defects of inanity still occur between the steel and concrete in the concrete-filled steel tubes. As far as the defects are inspected, the essential retrofit and repair are required which are normally expensive and time-consuming.

The finite element method has now been successfully used in simulation of the CFST columns as an alternative to experiments to understand the behavior of CFSTs. Schneider (1998) developed a 3-D nonlinear finite element model for circular concrete-filled steel tube columns. Hu *et al.* (2008) developed a nonlinear finite element model using the ABAQUS commercial package to simulate the behaviour of concrete-filled steel tube columns. In Hu's study, the concrete confinement was achieved by matching the numerical results by trial and error through parametric studies. Results from the finite element simulation will provide detailed information on the stress and the strain distributions in the composite members. Furthermore, the parametric studies on the finite element models can be performed to investigate the influencing factors to improve the structural efficiency.

The aim of this investigation was to study the axial loading behaviors for the CFST columns with separation gaps between the core concrete and the steel tube. A FE model was developed for the CFST columns with inanity defects. Numerical simulations were carried out by employing the nonlinear finite element method. The FE model was calibrated against the test data of the axially loaded CFST columns in terms of load-deformation curves as well as the failure modes. The different debonding gaps were then introduced, and influences of the debonding gaps on the behavior of the CFST columns were studied. Effects of the debonding gaps influenced by the parameters such as the strength of concrete, the yield stress of steel and the steel ratio, on the load carrying capacity of the axially loaded CFT columns in different conditions were also discussed.

## 2. Debonding model and debonding separation ratio

Debonding of the core concrete from the steel tube would be caused by the plastic shrinkage, the long term effect of the concrete as well as improper concrete casting. Normally, debonding caused by long term effect of concrete like shrinkage will introduce a separation gap of 1 to 3 mm at the steel concrete interface (Liu *et al.* 2011, Xue *et al.* 2010), which would certainly reduce the confinement effect to the core concrete. The inanity or separation gap of debonding induced by improper concrete casting would however cause a more severe gap between the steel tube and the core concrete. In convenience for analysis, a debonding separation ratio  $R_d$  is defined dividing the separation gap area by the whole cross sectional area of the CFST section and expressed as follows

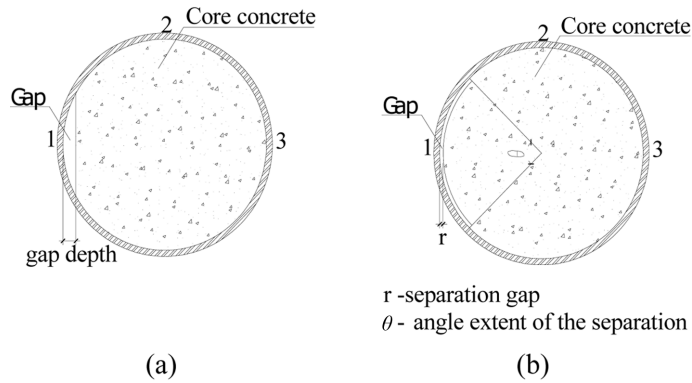


Fig. 2 Section of debonding model of a CFST section

$$R_d = \frac{A_d}{A_g} \tag{1}$$

where  $A_d$  is separation gap area and  $A_g$  is the gross cross sectional area of the CFST section. The dimensions and the notations of the debonding model of the CFST columns are illustrated in Fig. 2(a). A similar definition of the debonding separation is given by introducing the arc length and the thickness of the corresponding debonding separation gap as shown in Fig. 2(b).

It is likely that the defect of inanity or debonding separation would not occur uniformly along the axis of the column. To simplify the numerical analysis but also on the safety side, it is assumed that the debonding separation is distributed uniformly along the CFST column length. The debonding separation ratio  $R_d$  is used throughout the following study.

### 3. Finite element analysis and verification

#### 3.1 Finite element modeling

The main topic of the interest is to study the full range behavior of the composite columns with

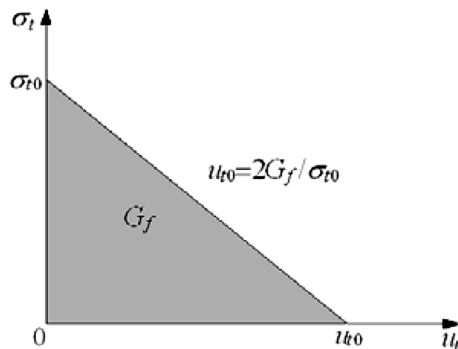


Fig. 3 Softening diagram of concrete in tension

different debonding separation gaps. The non-linear finite element analysis program ABAQUS was used to predict the load deformation behavior and the failure mode of the composite columns in axial compression.

Considering the double symmetric planes of the column, the finite element model was simulated for one quarter of the specimen. Symmetric boundary conditions were enforced on the symmetric planes, where the nodes were restrained perpendicular to these planes ( $x$ - $z$  plane and  $x$ - $y$  plane at the middle height of the column shown in Fig. 4(a)). Both material and geometric non-linearity was considered in the analysis and the Newton-Raphson iterative method was applied in the FE analysis solution using the displacement control technique to trace the loading paths.

The steel tube was modeled using the three-dimensional iso-parametric shell elements (S4R), which is defined by four nodes having three translational and three rotational degrees of freedom at each node. The concrete core of the column was modeled by the three-dimensional solid elements (C3D8R), which is defined by eight nodes having three translational degrees of freedom at each node, and is capable of cracking in three orthogonal directions, crushing in compression, plastic deformation and creep.

To ensure the loading equally distributed between the two materials, two thick steel caps were placed on top and bottom of the CFT column, and represented as rigid element body in the analysis. Fixed ends were achieved by restraining displacement and rotation against all degrees of freedom except in direction of the applied load. The load was applied in incremental step in the  $z$  direction using the modified RIKS method available in the ABAQUS library. For the axial loaded columns, the uniform compression displacement in the  $z$  direction was applied to the top cap. For the eccentric loaded columns, the displacement in the  $z$  direction was applied on the nodes along the loading line on the top cap which is on the same side of the debonding gap as shown in Fig. 4(c). The thick end caps were treated as the non-compression elastic material with an elastic modulus of  $E = 10^{12}$  N/mm<sup>2</sup>, and modeled using solid elements (C3D8R). The surface-to-surface contact was used between the core concrete and the steel caps.

The debonding area was simulated by the space between concrete and steel. To simulate the contact between the inner surface of the steel tube and the concrete core, in the surface of steel and concrete without debonding separation, the contact elements were used in the analysis. Penalty function was employed and the coefficient of friction,  $\mu$  between these faces was taken as 0.6. The friction is maintained as long as the surfaces remain in contact. Through the interface elements, the contact surfaces between the concrete and steel tube were allowed to separate although no penetration between each other was allowed.

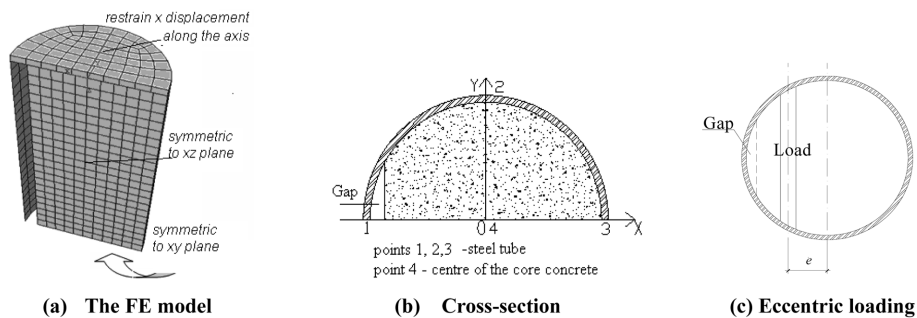


Fig. 4 A finite element model and cross-section of the column

Stress strain relation of the steel tube was treated as an isotropic elastic-plastic material and a tri-linear curve had been fitted to the experimentally obtained stress-strain curve. The Von Mises yield criterion and kinematics-hardening rule were used to define the behaviour of shell elements. The values of Young's modulus and Poisson's ratio of steel were taken as  $2.06 \times 10^5$  MPa and 0.3 respectively.

Concrete-filled steel tube circular columns with a small value of the  $D/t$  ratio would provide remarkable confinement for the concrete. A confined concrete model develop by Han *et al.* (2008) was used, and the equivalent uniaxial compression constitutional relationship is expressed as

$$y = \begin{cases} 2x - x^2 & (x \leq 1) \\ \frac{x}{\beta_0(x-1)^2 + x} & (x > 1) \end{cases} \quad (3)$$

where  $x = \varepsilon/\varepsilon_0$ ,  $y = \sigma/f'_c$ , and  $\varepsilon$  is the strain,  $\varepsilon_0$  is the peak compression strain value,  $\sigma$  is the stress,  $f'_c$  is the cylinder compression strength of concrete in N/mm<sup>2</sup>,  $\beta_0 = (2.36 \times 10^{-5})^{[0.25 + (\xi - 0.5)^2]} \times f'_c{}^{0.5} \times 0.5 \geq 0.12$ , and the confined ratio is defined as  $\xi = A_s f_y / A_c f_{ck}$ , where  $A_s$  and  $A_c$  are the sectional areas of the steel tube and the concrete core respectively,  $f_y$  and  $f_{ck}$  are the yield stress of steel and the characteristic cylinder compression strength of concrete respectively.

Softening effect was considered for concrete in tension and it obeys the stress-strain curve in a term of fracture energy of concrete denoted in  $G_f$ , an option provided by ABAQUS, as shown in Fig. 3.

### 3.2 Verification of the finite element analysis

To verify the finite element model, a comparison between the experimental results and finite element results was carried out. Three composite columns, PX-0-0, PX-50-0 and PX-50-5 tested by Liang (2008) were chosen for the initial verification. The specimens are CCFST columns (circular concrete filled steel tubes) subjected to axial loading. The specimens are denoted by two digital numbers, in which the first number represents for eccentricity of the applied load to the centroid of the cross-section, and the second number represents for the separation gap depth as defined in Fig. 2, for example specimen PX-0-0 is the CST column without separation gap at the interface between the steel tube and the core concrete, specimen PX-50-0 is the column without separation gap but is subjected to an eccentric axial load at 50 mm from the centroid, and specimen PX-50-5 is the column with separation gap of 5 mm and is subjected to an eccentric axial load.

The dimensions and material properties of the specimens are given in Table 1, in which,  $f_{cu}$ ,  $f_y$  and  $f_u$  are the cube strength of concrete, the yield stress and the ultimate tensile strength of steel respectively,  $L$  is the length of the column,  $D$  is the diameter of column,  $t$  is the thickness of steel tube,  $e/r$  is the eccentricity, of the applied compression load,  $r$  ( $D/2$ ) is the radius of column and  $R_d$  is the debonding separation ratio as defined in Eq. 1.

In construction practice, debonding separation depth would vary along the axis of the columns, for a typical case, the measured separation depth varies from 1.3 mm to 3.5 mm along the axis of the columns (Liu *et al.* 2011, Xue *et al.* 2010). Simplifying the analysis approach of the problem, a unified depth of the separation gap along the axis was assumed, however the bearing capacity evaluation should be on the safe side.

The cross-section of the columns and the FE model are illustrated in Fig. 4, where points 1, 2, and 3 are positioned at the steel tube section, and point 4 locates at the concrete core. The material and geometric properties of each specimen are listed in Table 1.

Table 1 Dimensions and material properties of the tested specimens

Specimens	$D \times t \times L$	$e/r$	$L/D$	$f_{cu}$ : MPa	$f_y$ : MPa	$f_u$ : MPa	gap depth: mm	$R_d$
PX-0-0	219×6×700	0	3.2	30.1	371.3	547.2	0	0
PX-50-0	219×6×700	0.457	3.2	30.1	371.3	547.2	0	0
PX-50-5	219×6×700	0.457	3.2	30.1	371.3	547.2	5	1%

The FE calculation results were compared with the test results, and good agreement had been achieved. Fig. 5 illustrates the relations between axial and transverse strains varying with the applied load for the steel tube and core concrete of the column (PX-0-0). Fig. 6 illustrates the corresponding load-strain curves for the column (PX-50-0). Fig. 7 illustrates the corresponding load strain curves for

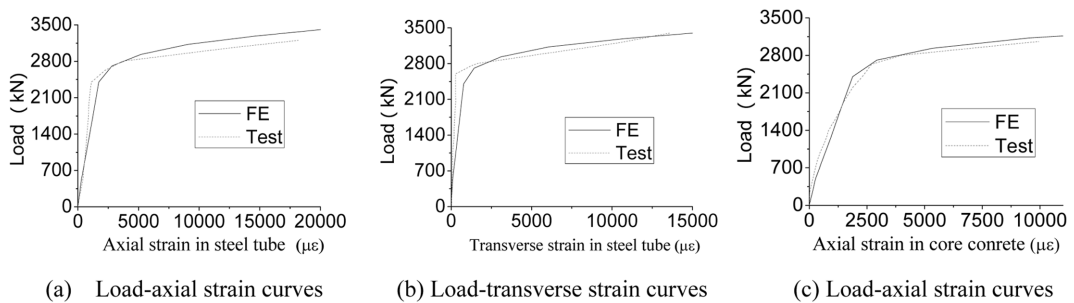


Fig. 5 A comparison of the FE results with the experimental results for specimen PX-0-0

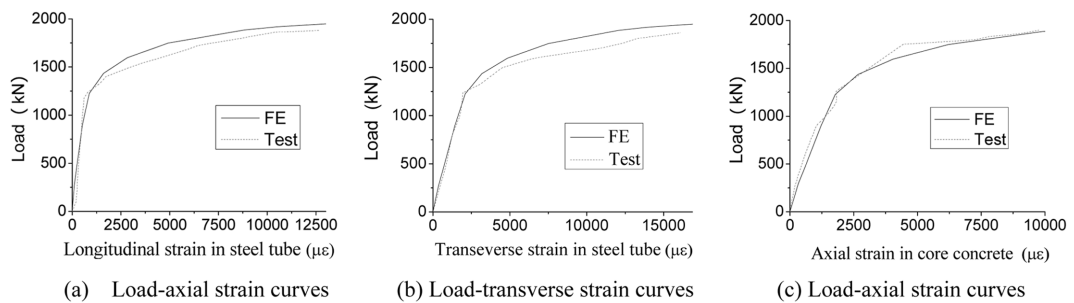


Fig. 6 A comparison of the FE results with the experimental results for specimen PX-50-0

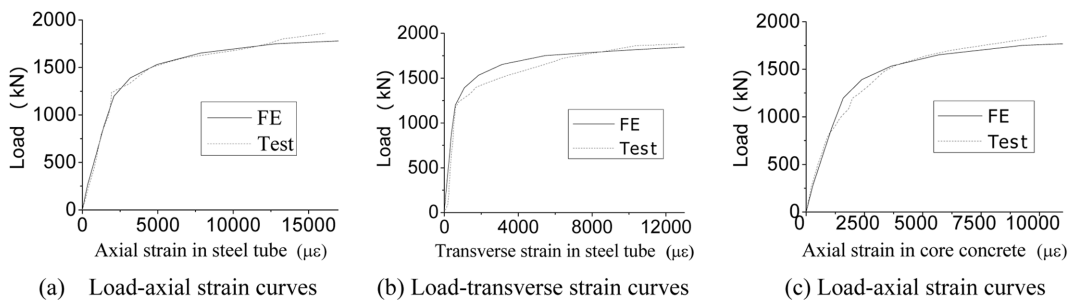


Fig. 7 A comparison of the FE results with the experimental results for specimen PX-50-5

the column with a unified separation gap of 5 mm at the steel-concrete interface (PX-50-5).

It is observed that the finite element model successfully predicts the ultimate load of the columns and the load–axial strain (or shortening) behavior. Both the elastic and the inelastic behaviors of the composite columns were predicted closely to the test curves, and the FE results correlated well with test results for the composite columns with and without debonding gaps. The FE models were verified in a good agreement with the test results in terms of the peak load and the load-strain curves for the steel and the core concrete.

It is worth noting that only the strain gauge’s readings rather than deformation from the LVDTs were plotted and compared. This is because that the early deformation observed and recorded near the capped ends during the tests did not exclude rigid displacement, which might not reflect the true deformation of the columns. It is also suggested that the use of the uniaxial confined concrete model (as expressed in Eq. (1) is justified for both the columns with and without debonding separation gaps.

#### 4. Parametric study

Further finite element analysis was carried out to study the behavior of the axial loaded composite columns being influenced by the debonding separation at the steel-concrete interface. The base specimen was a CCFST column with  $D = 574$  mm,  $t = 12$  mm,  $L = 2200$  mm,  $f_y = 345$  N/mm<sup>2</sup> and  $f_{cu} = 60$  N/mm<sup>2</sup> (cube strength). Length to diameter ratio ( $L/D$ ) of the specimens was 3.8 so that the overall buckling did not govern the strength of the columns.

The local slenderness ratio ( $D/t$ ) of the steel tube was less than a value of 90 ( $235/f_y$ ) which is equal to 90 (for  $f_y = 235$  N/mm<sup>2</sup>) and 61 (for  $f_y = 345$  N/mm<sup>2</sup>), to exclude influence of the local buckling. Seven cases of different separation gaps, with the denoted separation gap ratios given in Table 2, were investigated.

Fig. 8 shows the mean axial strain varying with the axial load for each specimen. The mean axial

Table 2 Separation gap depth and separation ratio of the specimens in the case study

gap depth (mm)	0	5	10	20	30	42.5	55
separation ratio	0	0.147%	0.414%	1.16%	2.13%	3.56%	5.2%

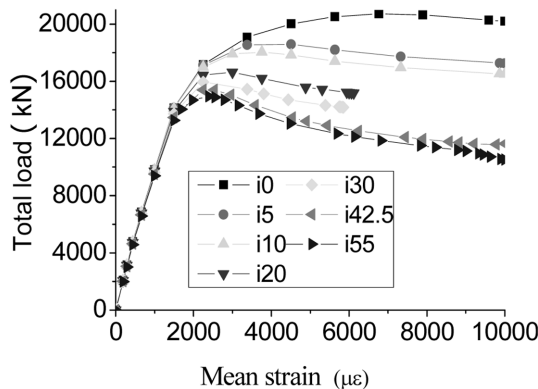


Fig. 8 Load vs. mean axial strain with different separation gap depth

strain was derived from the axial shortening divided by the length of the specimen. The notation  $i_0$  defined in the Fig. 8 represents a separation gap of zero, while  $i_5$  and  $i_{30}$  represent separation gap depth of 5 mm and 30 mm respectively. In the elastic range, each column behaved almost the same, while differential features occurred in the post peak and in the nonlinear stage. It appears that the axial load capacity of a CCFST column decreased when the separation gap depth increased. The axial forces shared by the core concrete and the steel tube were then drawn against the mean axial strain for each specimen as shown in Figs. 9 and 10.

Fig. 9 illustrates the load shared by the core concrete varying with the mean axial strain. It is found that the axial force at the ultimate state shared by the core concrete would reduce when the separation gap increased from 0 to 55 mm.

This could be explained owing to the less confinement to the core concrete of the steel tube in the cases of more separation gap, hence less extra strength developed in the core concrete. In existence of the separation gaps, the composite columns behaved likely eccentrically loaded, and the axial strains did not uniformly distribute across the cross section. The eccentricity also appeared increasing with the separation gaps. The ultimate force shared by the steel tube is however kept almost the same for each specimen as shown in Fig. 10.

Fig. 11 shows variations of the confined stress of the steel tube to the core concrete at position 2 and

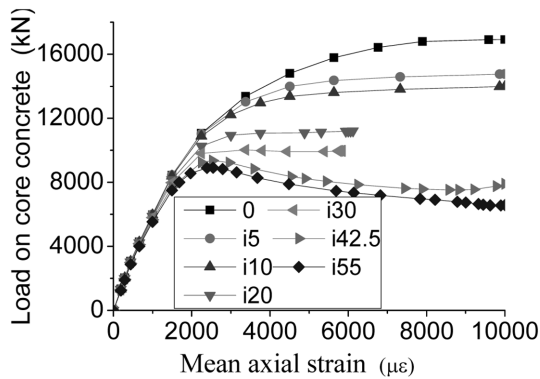


Fig. 9 Load shared by the core concrete varying with the axial strain curves in different separation gap ratios

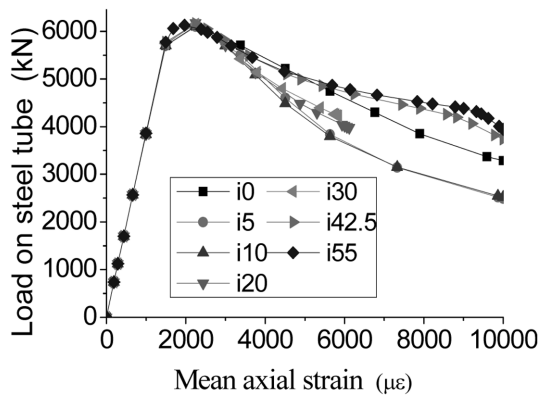


Fig. 10 Load shared by the steel tube varying with the axial strain curves in different separation gap ratios

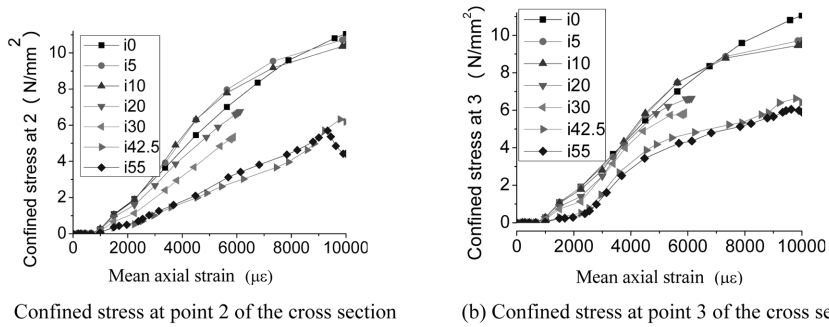


Fig. 11 Confined stress to the core concrete varying the mean axial strain in different separation gap ratios

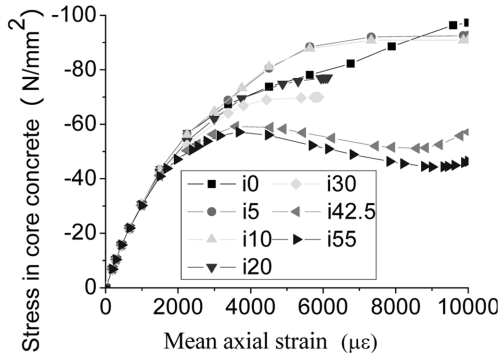


Fig. 12 Axial stress-strain curves for the core concrete influenced by separation gap ratios

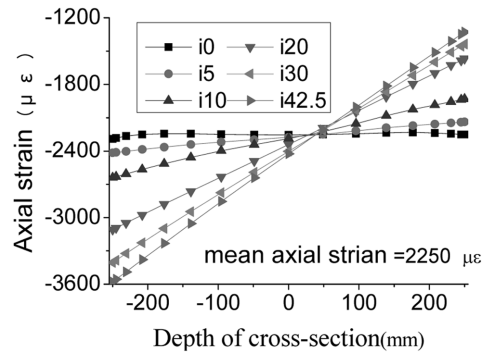


Fig. 13 Strain distribution over the cross sections influenced by separation gap ratios

position 3 for each specimen with different separation gap depths. The developed confined stress tends to decrease when the separation gap increased in the later post yielding stage of the curves.

The confined effects on the core concrete strength are illustrated in Fig. 12 varying with the separation gap. The strain corresponding to the peak compression stress likely reduced when the separation gap increased. The peak stress at the center of the core concrete also decreased sharply when the separation gap increased. The confinement enhancing effect on the core concrete also decreased when the separation gap increased, for the typical cases, when the gap depth was greater than 30 mm.

Stressing eccentricity of the cross section would be induced in the columns in existence of debonding separation gaps as shown in Fig. 13. Fig. 13 illustrates the axial strains distributed over the cross sections in different separation gaps. For the column without separation gap, the strain distributed uniformly across the cross-section, while non uniform distributed strain occurred when separation gaps existed at the interface between the steel tube and the core concrete. The more separation gap, the more eccentric deformation would occur.

Fig. 14 illustrates the axial stress distributions over the concrete section under different separation gaps, when the mean axial compression strain was 2250  $\mu\epsilon$ . Briefly, the composite columns with separation gap likely behaved as eccentrically loaded columns. The confined action of steel tube to the core concrete tended to decrease as the separation gap increased, leading to reduction in the axial load capacity of the composite columns.

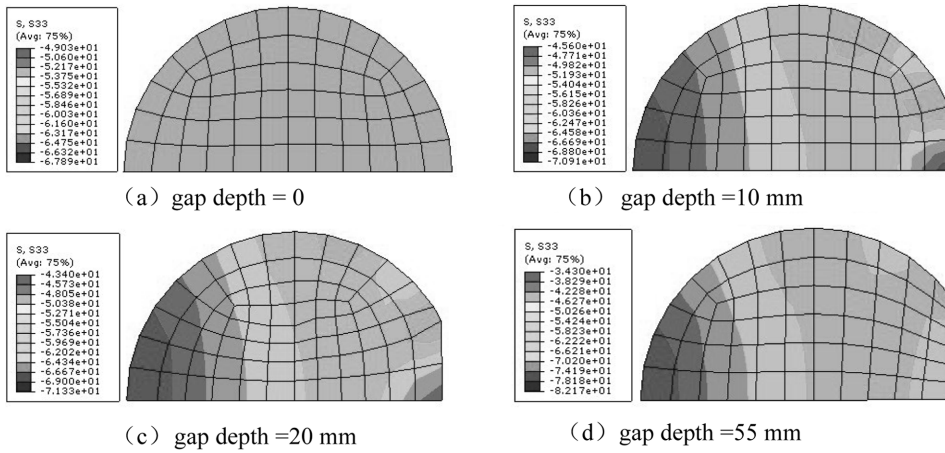


Fig. 14 Axial stress distribution over the concrete section under different separation gaps when the mean axial strain equals to 2250  $\mu\epsilon$

Influences of the steel ratio, the steel yielding strength and the compression strength of the core concrete on behaviours of the CCFST columns were further investigated. A series of 35 CCFST composite columns in five groups of with different steel tube thickness and seven cases of separation gap depth for each group were analyzed. Diameter of the cross-section for each specimen was 574 mm, while thickness of the steel tubes of the columns was 8, 10, 12, 16 and 20 mm respectively. The length, the yield stress of steel and the strength of the core concrete were the same as those of the base specimen studied previously. The seven designated separation gap ratios as listed in Table 2 were 0, 0.147%, 0.414%, 1.16%, 2.13%, 3.56% and 5.2% corresponding to a gap depth from 0 to 55 mm respectively.

In terms of the axial load capacity evaluation, two nominal base ultimate strengths, namely  $N_0$  and  $N_u$  are used, where  $N_0 = f'_c A_c + f_y A_s$  is the axial load strength derived from simple superposition of the steel tube and the concrete core, in which  $f'_c$  is cylinder strength of the concrete,  $f_y$  is the yielding strength of steel tube,  $A_c$  and  $A_s$  are the cross-section areas of the concrete core and the steel tube respectively, and  $N_u$  is the ultimate strength of the composite column without separation gap based on the FE analysis results. The dimensionless ratios and of each group of specimens are drawn against the separation gap ratio as shown in Figs. 15(a) and (b). One can find that under the same separation gap, the thicker the steel tube, the greater the axial load capacity or  $N/N_0$ . As shown in Figs. 15(a) and (b), increasing the steel tube thickness enhanced the confinement of steel to the core concrete, so increasing the axial load strength of the columns. It appears that  $N/N_0$  was smaller than 1.0 when the separation gap ratio was greater than 1%, and this value decreased to 0.8 when the separation gap ratio was up to 5%. Compared with the ultimate load capacity  $N_u$  of the perfected CCFST column (without debonding separation), reducing steel tube thickness also led to a drop in  $N/N_u$  as illustrated in Fig. 15(b).

Influence of concrete strength to the composite columns with the debonding separation is illustrated in Fig. 16. Three grades of concrete strength adopted were C40, C50 and C60, corresponding to the concrete with a cube strength of 40, 50 and 60 MPa respectively. Similar declining tendency in the axial load carrying capacity is observed when the separation gap increases. It is illustrated that under the same separation gap, increase of concrete strength led to decrease in  $N/N_0$ .  $N/N_0$  was less than 1 when separation gap ratio was greater than 1% and this value dropped to 0.8 if the separation gap ratio was up

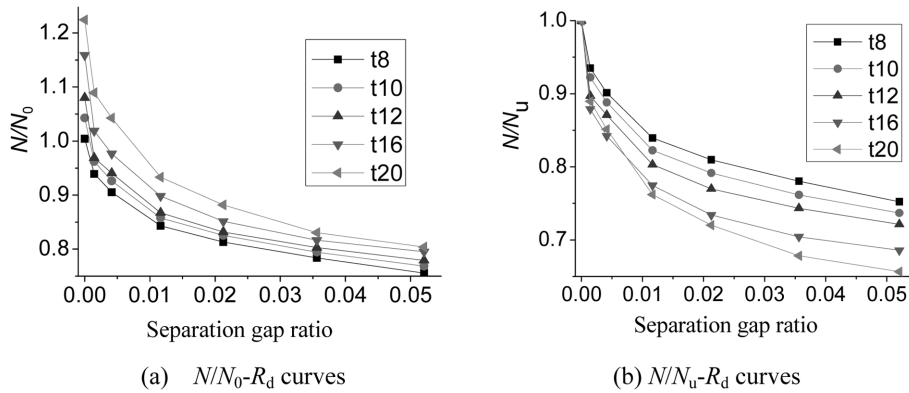


Fig. 15 The axial load capacity influenced by separation gap ratios in different steel ratios

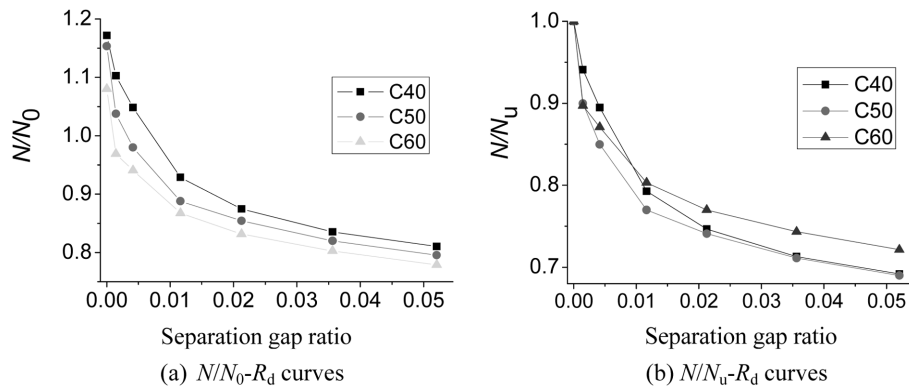


Fig. 16 The axial load capacity influenced by separation gap ratios in different concrete strength

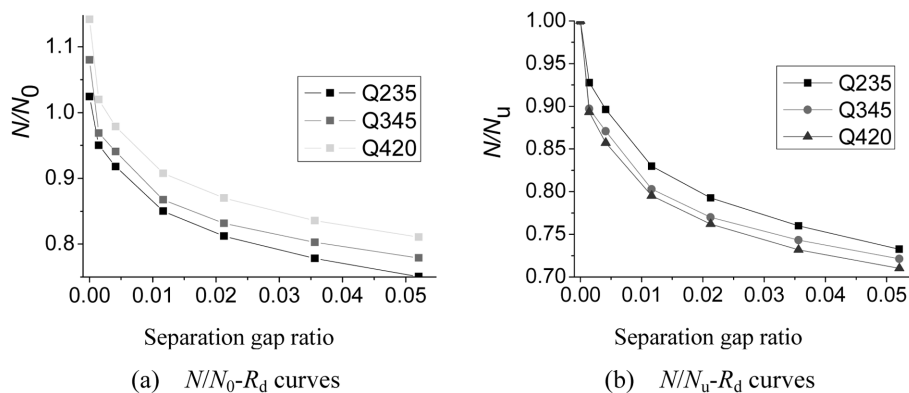


Fig. 17 The axial load capacity influenced by separation gap ratios in different yield stress of steel tube

to 5%. The enhancing effect on the axial load carrying capacity was found decrease when concrete strength increases in existence of the separation gap.

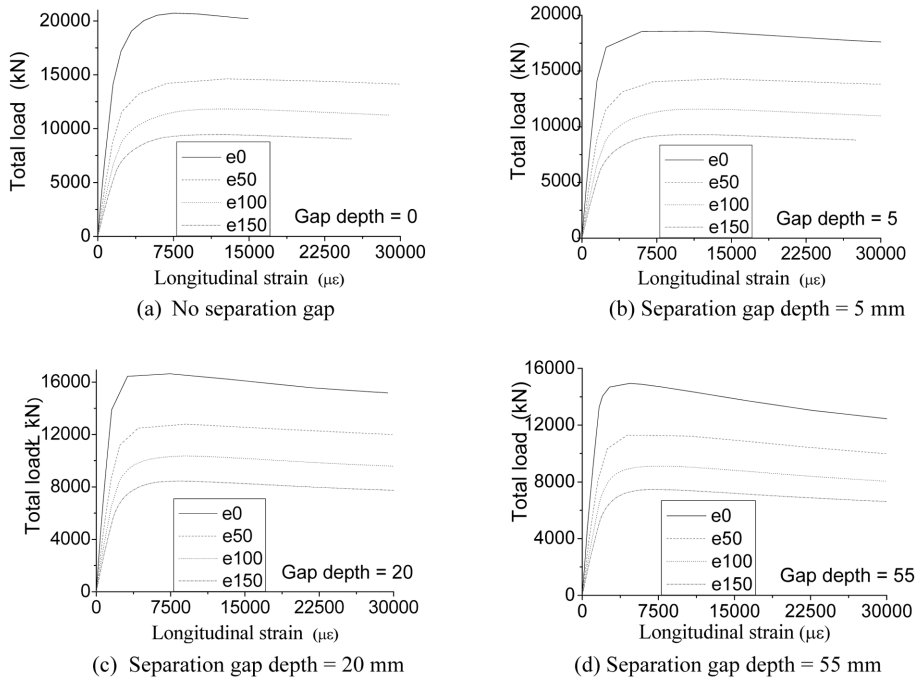


Fig. 18 Load-axial strain curves of specimens with different axial load eccentricities

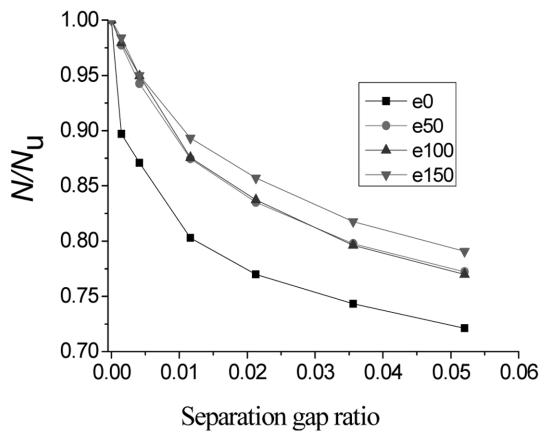


Fig. 19 Load reduction ratios varying with separation gap ratio (FE study)

Three yield stresses of the steel tube have been studied, and influence of the yield stress of steel tube to the composite columns is shown in Fig. 17. Increase in yield stress, increases  $N/N_0$  ratio. Similar tendency of  $N/N_0$  was found that  $N/N_0$  was less than 1 when separation gap ratio was greater than 1% and this value dropped to 0.8 when the separation gap ratio was up to 5%.

Influence of the axial load eccentricity was also analyzed. Four cases of the eccentric axial load (as shown in Fig. 3) were studied. Eccentricity of the axial load is 0, 50, 100 and 150 mm respectively, corresponding to the axial eccentricity ( $2e/D$ ) of 0, 0.174, 0.348 and 0.523. The load against the axial

strain is plotted in Fig. 18.

It is clearly shown that the axial load capacity decreases as the eccentricity of the axial load increases for the all separation gap cases. Fig. 19 plots ratio of  $N/N_u$  varying with the separation gap ratio in different axial load eccentricities. In the concentric loaded columns (the curve notated by e0), the drop of  $N/N_u$  influenced by the separation gap appears more significantly than those of the eccentric loaded columns (curves e50, e100 and e150) as shown in Fig. 19.

## 5. Discussions

In design practice, different methods have been used to assess the ultimate axial capacity of a concrete-filled steel tube circular column. It is generally considered that the American Specifications and the Australian Standards (ACI/AS) are conservative in calculating the design strengths for the CCFST columns, since neither of these specifications takes into consideration the concrete confinement. As shown in Figs. 15, 16 and 17, the predicted ultimate axial load capacities of the CCFST specimens are all greater than that derived by simple strength superposition of the steel tube and the core concrete when no separation gap occurs at the steel concrete interface. The EUROCODE 4 takes into account the concrete confinement by the circular steel hollow sections by introducing two parameters like  $\eta_1$  and  $\eta_2$ , and the axial capacity of a CCFST column is expressed as

$$N_{EC4} = A_s f_y \eta_2 + A_c f_c \left( 1 + \eta_1 \frac{t f_y}{D f_c} \right) \quad (4)$$

where  $A_s$  is the cross-sectional area of the steel tube,  $A_c$  is the cross-sectional area of the concrete and  $\eta_1$  and  $\eta_2$  are coefficients of confinement for concrete and steel tube, respectively.

The dissimilarities between these specifications are likely owing to the presumed assumption of the perfect interaction at the interface between the core concrete and the steel tube. Debonding separation and separation gaps would influence the ultimate strength of these composite members. The previous analysis has demonstrated that the ultimate axial load is reduced when the separation gap increases. As the ratio of length to diameter and the ratio of diameter to thickness were limited, the specimens were generally not governed in buckling failure. Reduced confinement effect should play the main role in the load capacity deterioration, although the reduced cross section area of the core concrete would contribute to decline of the bearing capacity, it should be very limited since the reduced area caused by the separation gap was much smaller than the rate of the declined load. Though the same confined concrete model was used in the FE analysis, the reduced confinement should be caused by separation gap, and the confined stress did not uniformly distribute in the cross section of the core concrete.

In the numerical study, a separation gap depth is assumed uniformly distributing over the length of the member as shown in Fig. 2(a). The debonding separation would more likely occur over the arc-length like the way as shown in Fig. 2(b). Tests were carried out by Xue *et al.* (2010) to investigate the influence of the debonding on the ultimate load capacity of the CCFST columns. The specimens were specially designed introducing debonding by inserting a galvanized sheet in the steel tube before the concrete casting and pulling it out 5~6 hours after the casting. A thickness of 2 mm was used for the separation gap in the study while the debonding arc length varied. The test results of  $N/N_u$  are plotted against the separation gap ratio, and the ultimate axial load is also found decreasing when the separation gap ratio  $R_d$  increases as shown in Fig. 20. In Fig. 20,  $A_s/A_c$  is known as the confinement ratio. In the same separation gap,  $N/N_u$  appears to decrease with higher confinement ratio. It implies that with the

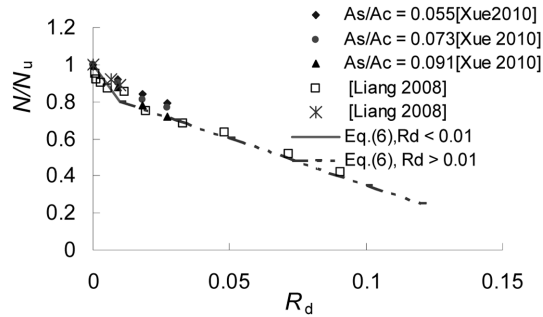


Fig. 20 Load reduction ratios varying with debonding separation (test study)

increase of the confinement ratio, the reduction coefficient of ultimate load capacity decreases.

Debonding separation of concrete from the steel tube would be still caused by either plastic shrinkage or long term effect of concrete like temperature, shrinkage even when improper concrete casting is controlled. It should be restricted if the concrete confinement is expected in assessment of the axial load capacity for the CCFST columns, and the load capacity of the CCFST columns has to be factored if the debonding separation is detected. This should be an alternative to the simply retrofitting the columns which is normally expansive.

Respective to the influence of the separation gap in the CCFST members, a reduction factor in the ultimate load capacity ( $K_D$ ) is defined as

$$K_D = \frac{N_D}{N_{u0}} \quad (5)$$

where  $N_D$  is the factored axial load capacity of a CCFST column in respective to separation gap,  $N_{u0}$  is the axial load capacity of the perfect CCFST column without separation gap.

For a concentric loaded composite column under different separation gap ratios,  $K_D$  is proposed as

$$\begin{aligned} K_D &= 1.0 - 20R_d & \text{if } R_d \leq 0.01 \\ K_D &= 0.85 - 5R_d & \text{if } R_d > 0.01 \end{aligned} \quad (6)$$

The prediction of  $K_D$  based on Eq. (6) is shown in Fig. 20. For an eccentric loaded column, eccentricity should be introduced in assessing the influencing factor, as shown in Fig. 19. A similar simplified calculation formula of  $K_D$  is proposed by Xue *et al.* (2012) more recently, in assessing the ultimate load capacity of circular CCFST columns with debonding when the column is subjected to axial load or small eccentric load. Further research should be required to clarify and assess the influence of the large eccentricity of axial loading.

## 6. Conclusions

The present study is an attempt to analyze the loading behaviours of the CFST members influenced by debonding separation at the steel concrete interface. A finite element model of the composite columns with the introduced debonding gap has been developed and was calibrated against experimental results. A series of parametric studies were conducted to investigate the ultimate strength of the

composite members with different separation gap depth, concrete strength, steel yield stress and the load eccentricity. Conclusions are drawn as follows:

1. Less confinement to the core concrete occurs in the cases when debonding separation occurs. The confinement enhancing effect on the core concrete decreases when the separation gap increases, and the axial load capacity of the CCFT column also decreases when the debonding separation gap increases.
2. In existence of the debonding separation, the axial strains do not uniformly distribute over the cross section, and the concentric loaded CCFST composite columns behave like an eccentric loaded member. The more debonding separation occurs, the more eccentricity is in the cross section.
3. Increase of the steel tube thickness enhances the confinement of steel to the core concrete, hence increase the axial load strength of the columns. Under the same debonding separation, increase in concrete strength will decrease  $N/N_0$  and increase in yield stress of the steel tube, however will increase  $N/N_0$ .
4. The axial load capacity decreases when the eccentricity of the axial load increases for the all separation gap cases. In the concentric loaded columns, drop of  $N/N_u$  influenced by debonding separation appears more significantly than that in the eccentric loaded columns.
5. Debonding separation should be restricted if the concrete confinement is expected in assessment of the axial load capacity for the CCFST columns. As an alternative to the simply retrofitting the composite columns, the load capacity of the CCFST columns has to be reduced if the debonding separation is detected.

## Acknowledgments

The authors appreciate greatly the National Science Foundation for the support of this research under the Grant No. 51078290, and the support from the Kwang-Hua Fund from the College of Civil Engineering, Tongji University. The cooperation and assistance of many people from the organization are greatly acknowledged.

## References

- American Concrete Institute (ACI), Building code requirements for structural concrete and commentary. ACI Committee 318-11, Michigan, 2011.
- American Institute of Steel Construction (AISC), Specification for Structural Steel Buildings (ANSI/AISC 360-10). Illinois, 2010.
- Architectural Institute of Japan (AIJ), Recommendations for design and construction of concrete filled steel tubular structures. Tokyo, 1997.
- Bahrami, A., Wan Badaruzzaman, W.H. and Osman, S.A. (2011), "Nonlinear analysis of concrete-filled steel composite columns subjected to axial loading", *Struct. Eng. Mech.*, **39**(3), 383-398.
- Choi, K.K. and Xiao, Y. (2010), "Analytical studies of concrete-filled circular steel tubes under axial compression", *J. Struct. Eng.*, **136**(5), 565-573.
- Ellobody, E., Young, B. and Lam, D. (2006), "Behavior of normal and high strength concrete-filled compact steel tube circular stub columns", *J. Constr. Steel Res.*, **62**(6), 706-715.
- Eurocode 4 (EC4). Design of steel and concrete structures-Part1-1:general rules and rules for building. EN 1994-1-1: 2004. Brussels, European Committee for Standardization. 2004.
- Gupta, P.K., Sarda, S.M. and Kumar, M.S. (2007), "Experimental and computational study of concrete filled steel tubular columns under axial loads", *J. Constr. Steel Res.*, **63**(2), 182-193.

- Hajjar, J.F. (2003), "Concrete-filled steel tube columns under earthquake loads", *Progress in Structural Engineering and Materials*, **3**(2), 72-81.
- Han, L.H., Liu, W. and Yang, Y.F. (2008), "Behavior of concrete-filled steel tubular stub columns subjected to axially local compression", *J. Constr. Steel Res.*, **64**(4), 377-387.
- Han, L.H. and Yao, G.H. (2003), "Influence of concrete compaction on the strength of concrete-filled steel RHS columns", *J. Constr. Steel Res.*, **59**(6), 751-767.
- Han, L.H. and Li, W. (2011), "New development on concrete filled steel Tubular (CFST) structures in China", *Proceedings of the 2011 World Congress on Advances in Structural Engineering and Mechanics (ASEM'11+)* Seoul, Korea, September.
- Hu, H.T., Huang, C.S., Wu, M.S. and Wu, Y.M. (2003), "Nonlinear analysis of axially loaded concrete-filled tube columns with confinement effect", *J. Struct. Eng.*, **129**(10), 1322-1329.
- Liang, K.F. (2008), "Research on the behaviors of concrete-filled steel tube with gaps under load", [D]. *PhD thesis of Hunan University*, Hunan China.
- Liang, Q.Q. and Fragomeni, S. (2010), "Nonlinear analysis of circular concrete-filled steel tubular short columns under eccentric loading", *J. Constr. Steel Res.*, **66**(2), 159-169.
- Liu, X.P., Sun, Z., Huang, H.Y., Tang, S. and Tang, C.H. (2011), "Research on mechanical properties of separation concrete-filled steel tubes Subjected to eccentric compression on non-separation side", *Appl. Mech. Mater.*, **117-119**, 887-892.
- Mu, T., Fan, B. and Xie, B. (2007), "Influence of de-fill on performance of concrete-filled steel tubular columns", *Proceedings of the 5th International Conference on arch bridges*, Madeira, Portugal, September.
- Roeder, C.W., Cameron, B. and Brown, C.B. (1999), "Composite action in concrete filled tubes", *J. Struct. Eng.*, **125**(5), 477-484.
- Schneider, S.P. (1998), "Axially loaded concrete-filled steel tubes", *J. Struct. Eng.*, **124**(10), 1125-1138.
- Uy, B. (1998), "Concrete-filled fabricated steel box columns for multistory buildings", *Progress in Structural Engineering and Materials*, **1**(2), 150-158.
- Uwe, S., Nabil, F. and Thomas, L. (2010), "Numerical analyses of the force transfer in Concrete-Filled Steel Tube columns", *Struct. Eng. Mech., An Int'l Journal*, **35**(2), 241-256.
- Xu, T.F., Xiang, T.Y., Zhao, R.D. and Zhan, Y.L. (2010), "Nonlinear finite element analysis of circular Concrete-Filled Steel Tube structures", *Struct. Eng. Mech., An Int'l Journal*, **35**(3), 315-333.
- Xue, J.Q., Chen, B.C. and Briseghella, B. (2010), "Experimental research on debonding in concrete-filled steel tubes columns subjected to eccentric loading", *IABSE Symposium Report*, IABSE Symposium, Venice.
- Xue, J.Q., Briseghella, B. and Chen, B.C. (2012), "Effects of debonding on circular CFST stub columns" *J. Constr. Steel Res.*, **69**(1), 64-76.
- Yin, X.W. and Lu, X.L. (2010), "Study on push-out test and bond stress-slip relationship of circular concrete filled steel tube" , *Steel. Compos. Struct., An Int'l Journal*, **10**(4), 317-329.
- Zhong, S.T. (2006), "Application and research achievement of concrete filled steel tubular (CFST) structures in China", *Proceeding of the 8th International Conference on Steel-Concrete Composite and Hybrid Structures*, Harbin, China, 12-14 August.